Title
APPLICATION OF ANALYTICITY PROPERTIES TO THE NUMERICAL SOLUTION OF THE BETHE-SALPETER EQUATION

Author
Haymaker, Richard W.

Publication Date
1967-07-28

UCRL-17700

University of California

Ernest O. Lawrence Radiation Laboratory

APPLICATION OF ANALYTICITY PROPERTIES TO THE NUMERICAL SOLUTION OF THE BETHE-SALPETER EQUATION

Richard W. Haymaker

July 28, 1967

Berkeley, California

DISCLAIMER

Submitted to Physical Review

UCRL-17700
Preprint

UNIVERSITY OF CALIFORNIA

Lawrence Radiation Laboratory
Berkeley, California

AEC Contract No. W-7405-eng-48

APPLICATION OF ANALYTICITY PROPERTIES TO THE NUMERICAL SOLUTION OF THE BETHE-SALPETER EQUATION

Richard W. Haymaker

July 28, 1967

UCRL-17700

APPLICATION OF ANALYTICITY PROPERTIES TO THE NUMERICAL SOLUTION OF THE BETHE-SALPETER EQUATION*

Richard W. Haymaker†

Lawrence Radiation Laboratory
University of California
Berkeley, California

July 28, 1967

ABSTRACT

A new method of calculating phase shifts from the Bethe-Salpeter equations is presented. The differential equations is solved below threshold by using a variational method, and then the scattering amplitude is continued to the physical-scattering region using Padé approximants. The singularity structure of the Bethe-Salpeter partial-wave amplitude in its off-shell variables was studied to find the nearby singularities that could most strongly affect the continuation.

I. INTRODUCTION

The recent calculations of phase shifts for the Bethe-Salpeter equation[1] in the ladder approximation have demonstrated the practical use of the equation for the study of two-body scattering amplitudes. Schwartz and Zemach[2] used the Schwinger variational principle based on the integral equation which yielded a rapidly convergent sequence of approximations to the phase shifts. A mesh-point solution has also been achieved which in addition was applicable to the three-particle inelastic region.[3] As more difficult problems of higher dimensionality are attempted (e.g., the three-body problem), the disadvantages of both methods become apparent. The Schwinger method becomes increasingly difficult to set up, and the mesh-point method may require prohibitively large matrices.

A comparison of the bound-state calculation of Schwartz[4] with the calculation of phase shifts by Schwartz and Zemach[2] shows that less sophisticated methods suffice to solve the former problem. The reason is that the boundary conditions on the wave function can be easily imposed, and thus the differential equation can be used. In this paper we present a method of computing phase shifts by calculating the scattering amplitude below elastic threshold and continuing it to the scattering region. By calculating below threshold we avoid the problems of solving a singular integral equation for the phase shift.[3,5,6] The homogeneous matrix equations that arise in the Rayleigh-Ritz bound-state calculation[4] can be applied directly to the calculation of the scattering amplitude merely by introducing an inhomogeneous term. A variational

principle exists for the amplitude in this region, and we get accuracy comparable to the Rayleigh-Ritz calculation. Unfortunately the method breaks down in the scattering region and so a numerical analytic continuation procedure is employed to get the phase shifts.

We propose this method as a means of getting the low-energy behavior of the phase shift as a byproduct of a bound-state calculation. Although scattering lengths and effective ranges can generally be calculated with this method, the extrapolation is not necessarily stable enough to get good values for phase shifts at higher energies. We present the analytic continuation of two different functions that are equal at the extrapolated point where the phase shift is desired. The first is an off-mass-shell continuation which is the Bethe-Salpeter analog of the method Schlessinger and Schwartz[7] used for the Schrödinger equation. The second is a continuation of the on-mass-shell amplitude that was reported earlier in a letter.[8] The latter method was more successful, but both are included in this paper for the sake of comparison.

In Sec. II the singularity structure of the partial-wave T matrix is studied close to elastic threshold in order to determine how close singularities come to the extrapolated points. The convergence of our method of analytic continuation is expected to be slow close to branch points. In Sec. III we discuss the motivation for calculating below threshold and describe the numerical procedure. Finally in Sec. IV the methods of continuation and results are presented.

II. SINGULARITIES OF THE PARTIAL-WAVE AMPLITUDE

A. Integral Equation for T_ℓ .

Consider the Bethe-Salpeter equation for the scattering of two particles of mass m with four-momenta k_1, $k_2 \to k_1'$, k_2'. In the center-of-mass system the integral equation for the scattering amplitude is

$$T_\ell(k', k_0', k, k_0, \omega) = \left(\frac{2\lambda}{\pi}\right) B_\ell^{(1)}(k', k_0', k, k_0) + \left(\frac{2\lambda}{\pi}\right) \int_0^\infty dp \int_{-\infty}^\infty dp_0 \, B_\ell^{(1)}(k', k_0', p, p_0) \times G_\omega(p, p_0) \, T_\ell(p, p_0, k, k_0, \omega), \tag{2.1}$$

where

$$\omega^2 = -\frac{1}{4}(k_1 + k_2)^2 ,$$

$$k = |\underset{\sim}{k}_1 - \underset{\sim}{k}_2|/2 ,$$

and

$$k_0 = (k_1 - k_2)_0/2 . \tag{2.2}$$

In the ladder approximation, the interaction kernel for single-particle exchange of mass μ and the Green's function are respectively

$$B_\ell^{(1)}(k, k_0', k, k_0) = -Q_\ell\left(\frac{k^2 + k'^2 - (k_0 - k_0')^2 + \mu^2}{2kk'}\right), \tag{2.3}$$

and

$$G_\omega(p,p_0) = i[(p^2 - p_0^2 - \omega^2 + m^2 - i\epsilon)^2 - 4\omega^2 p_0^2]^{-1} . \qquad (2.4)$$

The on-mass-shell value of T is related to the phase shift through the formula

$$T_\ell(q,0,q,0,\omega) = -\left(\frac{2}{\pi}\right)^2 q\,\omega\, e^{i\delta_\ell} \sin\delta_\ell , \qquad (2.5)$$

where $q = (\omega^2 - m^2)^{\frac{1}{2}}$.

Our primary interest is to find the singularity structure of T_ℓ in the variable q close to elastic threshold.[9] There are two different continuations that are of interest for the numerical work that follows which govern the emphasis of this section. The first is a continuation in q from the bound-state region to the scattering region holding k equal to k' and at the point where the phase shift is desired. The second is again a continuationin q but with k and k' constrainted to the mass shell, i.e. $q = k = k'$. For both cases we have $k_0 = k_0' = 0$. In practice we must find the singularities for a much larger domain of these variables, since they are found by iterating the equation.

A large class of singularities are generated by Eq. (2.1) through pinches of the contours by singularities in the integrand. Their positions are functions of the momentum variables and masses but are independent of λ. By iterating the equation N times we get in operator form

$$T = \lambda B + \lambda^2 B G B + \cdots \lambda^{N+1} (B G)^{N+1} T . \qquad (2.6)$$

We will assume that T contains the singularities of all Born terms whether or not the Born series converges, i.e. that the singularities in the last term of Eq. (2.6) do not cancel the singularities of the first N Born terms. The nth Born term is given in terms of the $(n-1)$th Born term through the formula

$$B_\ell^{(n)}(k', k_0', k, k_0, \omega) = \int_0^\infty dp \int_{-\infty}^\infty dp_0 \; B_\ell^{(1)}(k', k_0', p, p_0) \, G_\omega(p, p_0) \times B_\ell^{(n-1)}(p, p_0, k, k_0, \omega) . \qquad (2.7)$$

There are of course also bound-state poles on the physical sheet of the ω plane for sufficiently attractive potentials. Their positions in ω will be independent of the momentum variables k, k', k_0, k_0' and can only be found numerically.

In Part B below we find all the singularities of the second Born term. In Part C we discuss the propagation of these singularities in successive Born terms through Eq. (2.7). Many singularities that we find are present in the full Feynman diagrams (not partial-wave-analysed) but are usually presented in the literature in terms of Lorentz-invariant variables. The transformation to our variables appropriate to the Bethe-Salpeter equation is

$$k_0^2 = (k_1^2 - k_2^2)^2/(16\omega^2),$$

$$k_0'^2 = (k_1'^2 - k_2'^2)^2/(16\omega^2),$$

$$k^2 = \omega^2 + \frac{1}{2}(k_1^2 + k_2^2) + (k_1^2 - k_1^2)^2/(16\omega^2),$$

and

$$k'^2 = \omega^2 + \frac{1}{2}(k_1'^2 + k_2'^2) + (k_1'^2 - k_2'^2)^2/(16\omega^2) . \qquad (2.8)$$

B. Singularities of the Second Born Term.

Let us consider $\ell = 0$ for the sake of clarity with no loss of generality. The second Born term is

$$B_\ell^{(2)}(k', k_0', k, k_0) = \frac{i}{2} \int_{-\infty}^{\infty} dp \int_{-\infty}^{\infty} dp_0 \log\left(\frac{S_3}{S_4}\right) \frac{1}{S_5 S_6} \log\left(\frac{S_1}{S_2}\right) . \qquad (2.9)$$

The integrand is singular on the surfaces $S_i = 0$, where

$$S_1 = (k - p)^2 - (k_0 - p_0)^2 + \mu^2$$

$$S_2 = (k + p)^2 - (k_0 - p_0)^2 + \mu^2$$

$$S_3 = (k' - p)^2 - (k_0' - p_0)^2 + \mu^2$$

$$S_4 = (k' + p)^2 - (k_0' - p_0)^2 + \mu^2$$

$$S_5 = p^2 - (p_0 - \omega)^2 + m^2$$

$$S_6 = p^2 - (p_0 + \omega)^2 + m^2 . \qquad (2.10)$$

The lower limit of the p integration was extended to $-\infty$ since the integrand is even in p.

These surfaces can trap the hypercontour and cause singularities in the external variables.[10] Since the integral is two-dimensional, one, two, or three of these surfaces can participate in trapping the hypercontour. It is clear that Formula (2.9) can be written as the sum of four terms each containing S_1 or S_2, and S_3 or S_4. Thus the interaction of S_1 and S_2, or S_3 and S_4 can produce no singularities. In that which follows we consider only the integral containing S_1, S_3, S_5, and S_6. It should be kept in mind that there are singularities due to three other integrals that can be found by appropriate replacements of $k \to -k$ and $k' \to -k'$ in the final results.

The conditions for a hyperpinch to occur in which m surfaces participate are:[10]

$$m = 1 \qquad S_i = 0, \qquad \frac{\partial S_i}{\partial p} = 0, \qquad \frac{\partial S_i}{\partial p_0} = 0 \; ; \tag{2.11a}$$

$$m = 2 \qquad S_i = 0, \; S_j = 0 \qquad \frac{\partial S_i}{\partial p} \frac{\partial S_j}{\partial p_0} = \frac{\partial S_j}{\partial p} \frac{\partial S_i}{\partial p_0}, \; i \neq j \; ; \tag{2.11b}$$

$$m = 3 \qquad S_i = 0, \; S_j = 0, \; S_k = 0, \quad i \neq j \neq k \neq i \; . \tag{2.11c}$$

The surfaces $S_i = 0$ are hyperbolas in the real p, p_0 plane as shown in Fig. 1a. The Feynman prescription of giving all internal masses a small negative imaginary part is used to remove all singularities

from the integration path and thus define the integrals. If we hold p fixed and real and look in the p_0 complex plane, the upper and lower branches of the hyperbolas in Fig. 1a lie respectively in the lower- and upper-half complex p_0 plane in Fig, 1b. Since the contour must be trapped at each stage of integration to produce a singularity in the integral it is clear that we need consider only those solutions in which an upper branch of a hyperbola pinches with a lower branch, for only these branches pinch in the p_0 integration.

We will examine in turn the solutions to Eqs. (2.11a,b,c) in which one, two, and three surfaces participate.

1. One Surface

First consider singularities generated by a single surface through Eq. (2.11a). These equations can be solved immediately and give singularities at $m^2 = 0$ and $\mu^2 = 0$. But since we are holding the masses fixed and finite, these solutions are not of interest.

2. Two Surfaces.

Next consider the interaction of two singular surfaces in producing singularities, Eq. (2.11b). For S_5 and S_6, these equations give the elastic threshold branch point at

$$\omega^2 = m^2 , \tag{2.12a}$$

and the well-known second-sheet branch point at

$$\omega^2 = 0 . \tag{2.12b}$$

These singularities occur in the box diagram and are shown in Fig. 2c.

These solutions have a nice pictorial interpretation in terms of Fig. 1a. The positions of the hyperbolas S_5 and S_6 are functions of the external variable ω. When a lower branch is tangent to an upper branch we get the hyperpinch at $\omega^2 = m^2$. When a lower (upper) branch is tangent to a lower (upper) branch we get the solution $\omega = 0$ but the hypercontour is not pinched. However, if we start at this solution and take ω on a path that encircles the branch point at $\omega = m$ once and return to $\omega = 0$, we will find that the p_0 contour is pinched.

Because of the special importance of the normal threshold to our analytic continuation, it is shown in the Appendix without relying on the Born series, that this pinch produces a two-sheeted "square-root type" branch point in the partial-wave amplitude.

The surfaces S_1 and S_3 generate the surfaces

$$(k - k')^2 - (k_0 - k_0')^2 + 4\mu^2 = 0 \qquad (2.13a)$$

and

$$(k - k')^2 - (k_0 - k_0')^2 = 0 . \qquad (2.13b)$$

The same considerations apply to the solution (2.13b) that were discussed above for Eq. (2.12b). Remembering that the masses have a small negative imaginary part, $-i\epsilon$, we can see this yet in another way. The solution (2.13a) gives a singularity for real values of all the variables only

when ϵ approaches 0, whereas the second solution, (2.13b), exists for real values of the variables for nonzero ϵ. However, we know that the integral is nonsingular for real values of these variables, the $-i\epsilon$ being introduced solely for that purpose.

The singularities due to S_1 and S_4, S_2 and S_3, and S_2 and S_4 follow immediately and are given in Table I.

Finally the last type of two-surface pinch is for example between S_1 and S_5 producing the surfaces

$$k^2 - (k_0 - \omega)^2 + (m + \mu)^2 = 0 \qquad (2.14a)$$

and

$$k^2 - (k_0 - \omega)^2 + (m - \mu)^2 = 0 . \qquad (2.14b)$$

Again we can discard the second solution. All the singularities of this type are summarized in Table I. It should be mentioned that these solutions are precisely the individual-particle normal thresholds given for the full Feynman graph in Fig. 2d expressed in the variables (2.8).

3. Three Surfaces

Finally there is the case in which three surfaces participate in trapping the contour. The simplest case is the combination S_1, S_5, and S_6, giving

$$(k - q)^2 - k_0^2 + \mu^2 = 0$$

and

$$(k + q)^2 - k_0^2 + \mu^2 = 0, \qquad (2.15)$$

where $q^2 = \omega^2 - m^2$. These solutions are just the "triangle singularity" corresponding to the contracted graph Fig. 2b in terms of the variables (2.8).

The sheet structure of this singularity in relation to the normal thresholds is not simple. But the work has been done for us to straighten out this structure[11] and we need only interpret the results in terms of our variables. This has been done and is shown in Fig. 3. This surface $T_{1,5,6}$ is tangent to the lower-order surfaces $T_{1,5}$ and $T_{1,6}$. If we pass along the surface $T_{1,5,6}$ from the solid portion, passing the point of tangency, the singularity goes onto the second sheet of the normal thresholds $T_{1,5}$ and $T_{1,6}$, shown in Fig. 3b.

The last and most complicated case is the three-surface pinch generated by the surfaces S_1, S_3, and S_5 :

$$[(k'^2 - (k'_0 - \omega)^2 + \mu^2 - m^2)(k_0 - \omega) - (k^2 - (k_0 - \omega)^2 + \mu^2 - m^2)(k'_0 - \omega)]^2$$

$$- [(k'^2 - (k'_0 - \omega)^2 + \mu^2 - m^2)k - (k^2 - (k_0 - \omega)^2 + \mu^2 - m^2)k']^2$$

$$+ 4m^2[k'(k_0 - \omega) - k(k'_0 - \omega)]^2 = 0 . \qquad (2.16)$$

Only this surface and the corresponding ones shown in Table I do not reduce to conic forms in the left-leg variables k'_0, k'. The key to picturing the surface $T_{1,3,5}$ is to look at its asymptotes in the k'_0, k' plane. This curve is asymptotic to the lines

$$(k_0' - \tilde{k}_0')^2 = (k' - \tilde{k}')^2 , \tag{2.17a}$$

where

$$\tilde{k}_0' = \omega + \frac{(k_0 - \omega)}{2} \Gamma \quad \text{and} \quad \tilde{k}' = \frac{k}{2} \Gamma , \tag{2.17b}$$

with

$$\Gamma = \left[1 \mp \left(\frac{k^2 - (k_0 - \omega)^2 + (m + \mu)^2}{k^2 - (k_0 - \omega)^2} \right)^{\frac{1}{2}} \right] . \tag{2.17c}$$

The important thing to note is that for the right-leg variables on the mass shell (i.e. $k = q$, $k_0 = 0$), these asymptotes are complex. One can also show that the surface does not intersect the real k', k_0' plane under these conditions. This situation persists for $k \neq q$ for those values of k and q of interest for the continuations we do.

The singularities of the second Born term are displayed in yet another way in Fig. 4. These are the relevant complex planes for the two numerical continuations. For both cases we have set $k_0 = k_0' = 0$. Fig. 4a shows the singularities in q for fixed $k = k'$, and Fig. 4b shows the analytic structure in the variable $q = k = k'$.

D. Iteration of Singularities in the Born Series.

With our knowledge of all the singularities of the second Born term $B_\ell^{(2)}(k', k_0', k, k_0, \omega)$ in the left-leg variables k', k_0', we could in principle find all the singularities of the third Born term using Eq. (2.7) and continue the process to find all singularities of the full partial-wave amplitude. To carry this out we must find the

singularities for unrestricted values of k' and k_0' at each stage, since they are integrated over in the next stage. For unrestricted values of k, k_0, and q the problem is quite difficult. In particular we know that all the singular surfaces of a Feynman N-rung ladder diagram with at least one rung contracted will not depend on $\cos\theta$ and thus will be present in the partial-wave amplitude.[12] The singularity structure of even this class of diagrams is poorly understood for general masses.

Most singularities of $B_\ell^{(2)}$ are hyperbolic surfaces in the integration variables p, p_0 (See Table I). This is a great simplification in that the complexity of the surfaces does not increase upon iteration. There are surfaces though that are not hyperbolic [Eqs. (12) and (13) of Table I]. However, for $k_0 = 0$ and $k = q$, they do not intersect the real k', k_0' plane and thus are not potent in producing pinches in higher Born terms for the hypercontour in the real p, p_0 plane. As mentioned earlier this situation persists for $k \neq q$ for the regions of interest.

Restricting ourselves to just the hyperbolic surfaces we can list a large class of singularities for $B_\ell^{(N)}(k', k_0', k, k_0, \omega)$ that depend on q (or ω). We list below those singularities that we believe are closest to the extrapolated region. We also include some singularities that are "far away" but arise in a simple manner.

(i) Normal thresholds in ω^2 :

$$4\omega^2 = (2m + \sigma\mu)^2 \qquad (2.18a)$$

$$q = -im . \qquad (2.18b)$$

(ii) Normal thresholds for each leg:

$$k^2 - (k_0 \pm \omega)^2 + [m + (\sigma + 1)\,\mu]^2 = 0 \qquad (2.18c)$$

$$k'^2 - (k_0' \pm \omega)^2 + [m + (\sigma + 1)\mu]^2 = 0\,. \qquad (2.18d)$$

(iii) Triangle-type singularities:

$$(k \pm q)^2 - k_0^2 + [(\sigma + 1)\,\mu]^2 = 0 \qquad (2.18e)$$

$$(k' \pm q)^2 - k_0'^2 + [(\sigma + 1)\mu]^2 = 0\,. \qquad (2.18f)$$

(iv) Singularities on the imaginary q axis:

$$q = -i\,\sigma\,\mu/2\,,\ (\sigma \geqslant 1)\,, \qquad (2.18g)$$

where $\sigma = 0, 1, \cdots, (N - 2)$.

The iteration appears to generate many more surfaces. A large class can be ruled out using the symmetry of $B_\ell^{(N)}(k', k_0', k, k_0, \omega)$ under $k \leftrightarrow k'$ and $k_0 \leftrightarrow k_0'$. There are many more triangle-type singularities, but just as the ones mentioned [Eqs. (2.18e,f)] are on the second sheet of the lowest threshold (see Fig. 5a), many of the others are on the second sheets of higher normal threshold. Figure 5 displays these singularities for the continuations of interest.

III. SOLUTION OF THE BETHE-SALPETER DIFFERENTIAL EQUATION

Our calculation of phase shifts is done in two stages. First the partial-wave amplitude is calculated at a set of energies below elastic threshold, using a variational method based on the differential equation. The amplitude is then continued to the scattering region, using the knowledge of its analytic structure dealt with in the previous sections. This section is devoted to the motivation for calculating below threshold and an outline of the methods used to calculate the input numbers for the continuation. We restrict ourselves to equal-mass scattering.

A. Wick Rotation and Asymptotic Behavior

The differential equation was solved for energy below threshold, because only there is it simple to impose the boundary conditions on the wave function at infinity in coordinate space. The wave function is exponentially damped in this region, and this is crucial for the application of our variational method.

The asymptotic behavior of the wave function can be found from the integral equation

$$\psi_{k,E}(x) = \psi_k^{o}(x) + \int d^4x'\, G_E(x - x')\, V(x')\, \psi_{k,E}(x'), \tag{3.1}$$

where

$$\psi_k^{o}(x) = e^{ik\cdot x}, \tag{3.2}$$

$$G_E(x - x') = -i \int \frac{d^4p}{(2\pi)^4}\, e^{ip\cdot(x-x')}\, G_\omega(p, p_o), \tag{3.3}$$

$$V(x) = \frac{4\mu\lambda}{|x|}\, K_1(\mu|x|), \tag{3.4}$$

and K_1 is the modified Bessel function. We have gone to the center-of-mass system and introduced the variable $E = 2\omega$ for convenience. As long as the integral converges, we see that the large x behavior is governed by the free-wave term and the Green's function. The free-wave term can be easily subtracted out, leaving the Green's function as our main concern.

It is well known that the Wick[13] rotation can be performed on the Bethe-Salpeter equation for E below threshold. This has the practical advantage of allowing the use of expansions in four-dimensional spherical harmonics in the subsequent work. Henceforth we will work with the rotated forms of the equations, where now all relative momentum vectors and coordinate vectors are Euclidean:

$$k = (\underset{\sim}{k}, k_4), \qquad x = (\underset{\sim}{x}, x_4)$$

$$k_4 = k_0 e^{-i\pi/2}, \qquad x_4 = x_0 e^{i\pi/2}. \tag{3.5}$$

Turning now to the integral representation of the Green's function in x space, Eq. (3.3), and holding $\omega^2 < m^2$, the Wick rotation can be carried out without passing any singularities. In the rotated form, the exponential components of the Green's function for large x are[14]

$$G_E(x) \sim \exp[i(\omega^2 - m^2)^{\frac{1}{2}} |\underset{\sim}{r}|] + \exp[\omega|x_4| - m R], \tag{3.6}$$

where $R = (|\underset{\sim}{r}|^2 + x_4^2)^{\frac{1}{2}}$. This clearly shows that for $\omega^2 < m^2$ on the

physical sheet, the Green's function is exponentially damped in all directions of the Euclidean four-space $(\underset{\sim}{r}, x_4)$, whereas for $\omega^2 > m^2$, the second term is a growing exponential in x_4. This reflects the fact that poles of $G_\omega(p, p_0)$ have moved into the first and third quadrants in Eq. (3.3) and have moved past the rotated p_0 contour on the imaginary axis.

The scattered part of the wave functions is also damped for $\omega^2 < m^2$ as long as the integral in Eq. (3.1) converges. For the off-mass-shell case in which ω and k are independent, the integral does indeed converge for the full region of ω stated. However, by going to the mass shell $E^2 = 4(k^2 + m^2)$, below threshold the free-wave term $\psi_k{}^0(x)$ in Eq. (3.1) becomes a real exponential. This exponential competes with the damped exponential under the integral giving only a finite region of ω where the scattered part of the wave function is exponentially damped. This effect signals the onset of the second Born contribution to the left-hand cut and will be discussed again below.

B. The Differential Equation

We can obtain the differential equation from the integral equation, Eq. (3.1) (where now all relative vectors are Euclidean), by operating on the equation with the differential operator with the property

$$\mathfrak{D}(\partial_\nu)\, G_E(x - x') = \delta^4(x - x') , \tag{3.7}$$

giving the wave-function equation in the center-of-mass system:

$$\mathcal{D}(\partial_\nu)\psi_{k,E}(x) = V(x)\psi_{k,E}(x) + \mathcal{D}(i\,k_\nu)\psi_k{}^0(x) , \tag{3.8}$$

where

$$\mathcal{D}(\partial_\nu) = [-\Box - (E^2/4) + m^2]^2 - E^2\left(\frac{\partial}{\partial x_4}\right)^2 \tag{3.9}$$

and

$$\Box = \sum_{\nu=1}^{4} \frac{\partial}{\partial x_\nu}\,\frac{\partial}{\partial x_\nu} . \tag{3.10}$$

The last term comes from the free-wave term in Eq. (3.1) and is zero for k_ν on the mass shell.

The scattered part of the wave function is

$$\chi_{k,E}(x) = \psi_{k,E}(x) - \psi_k{}^0(x) . \tag{3.11}$$

The differential equation for $\chi_{k,E}(x)$ is

$$\mathcal{D}(\partial_\nu)\chi_{k,E}(x) = V(x)[\chi_{k,E}(x) + \psi_k{}^0(x)] . \tag{3.12}$$

C. Variational Principle

A Kohn-type variational principle[15] based on the differential Eq. (3.12) that gives a stationary expression for T is

$$\begin{aligned}[T(k',\,k,\,E)] = {} & \int d^4x\, \chi^*_{k',E}(x)\,\{\mathcal{D}(\partial_\nu) - V(x)\}\chi_{k,E}(x) \\ & + \int d^4x\, \chi^*_{k',E}(x)V(x)\psi_k{}^0(x) + \int d^4x\, \psi_k{}^{0*}(x)V(x)\chi_{k,E}(x) \\ & + \int d^4x\, \psi_{k'}{}^{0*}(x)\, V(x)\psi_k{}^0(x) .\end{aligned} \tag{3.13}$$

This expression is stationary with respect to first-order variations of $\chi_{k,E}(x)$ about its true solution, and thus a first-order error in the wave function will give a second-order error in T :

$$\frac{\delta[T]}{\delta \chi^*} = 0 , \qquad \frac{\delta[T]}{\delta \chi} = 0 . \tag{3.14}$$

The last term of the variational principle is just the first Born term. This is considerably simpler to apply in practice than the Schwinger variational principle used by Schwartz and Zemach.[2]

This variational principle is an exact statement and holds for arbitrary k, k', and E. However, it may be that the integrals ostensibly diverge and have a meaning only through analytic continuation. Also when introducing a set of expansion functions for χ that are capable of representing the true wave function, it may well be that the matrix elements in such a basis will diverge. This happens for certain values of E, k, and k' and severely limits the applicability of this variational principle in practice. The off-mass-shell and on-mass-shell cases will be considered separately.

1. Off-Mass-Shell

For this case E is independent of k and k'. Fix k and k' to represent true scattering states: $k = (\underset{\sim}{k}, 0)$, $k' = (\underset{\sim}{k}', 0)$, $|\underset{\sim}{k}| = |\underset{\sim}{k}'|$. For $E^2 < (2m)^2$, $\chi(x)$ is a decaying exponential for large x which may be represented well by a set of trial functions with a decaying exponential behavior, and all the integrals in Eq. (3.13)

converge. For $E^2 > (2m)^2$, however, $X(x)$ contains a growing exponential component in x_4, and it defies ones imagination to find a simple set of trial functions with the growing exponential that will yield convergent integrals. The derivative term in Eq. (3.13) is the troublesome one; all other terms have a potential present which is a decaying exponential in all directions. A possible method of circumventing this difficulty is to introduce an integral representation of the wave function:

$$X_{k,E}(x) = \int d^4x' \, G_E(x - x')\varphi(x') \, . \qquad (3.15)$$

An examination of the integral equation for $X(x)$ shows that $\varphi(x)$ contains a decaying exponential in the elastic-scattering region. Using the property (3.7), we see that the derivative term is a convergent integral. But now we have integrals to evaluate of the same difficulty as those of the Schwinger method.[2]

2. On-Mass-Shell

The additional constraints $E = 4(|\underset{\sim}{k}|^2 + m^2) = 4(|\underset{\sim}{k}'|^2 + m^2)$ limit further the applicability of Eq. (3.13). The free-wave $\psi_k{}^0(x)$ which is oscillatory for the above case becomes a real exponential below threshold, and for $\mathrm{Im}(k) > \mu$ the integrals again diverge. Also at this point our estimate of the asymptotic behavior of $X(x)$ is no longer valid as discussed above. So finally the domain of applicability in E is $4(m^2 - \mu^2) < (2m)^2$. This is the region between the elastic threshold and the second Born contribution to the left-hand cut. (The first Born term was included explicitly.) These considerations might

suggest that the full amplitude has a singularity at $E^2 = 4(m^2 - \mu^2)$. Although the variational principle for the full amplitude breaks down at this point, only the partial-wave amplitude in fact has this singularity.

D. Numerical Method

To solve the Bethe-Salpeter equation we first introduce a linear parameterization of the wave function $\chi_{k,E}(x)$:

$$\chi_{k,E}(x) = \sum_{\substack{\ell=0 \\ n=\ell \\ j=n}} a_{\ell,n,j}\, \mathcal{Y}_{n\,\ell\,0}(\hat{x})\varphi_j(R)\,, \tag{3.16}$$

where $\mathcal{Y}_{n\,\ell\,m}$ are four-dimensional spherical harmonics on the four-sphere, and $\hat{x}$ is the unit four-vector in the Euclidean space. The four-dimensional spherical harmonics can be expressed in terms of the usual three-dimensional spherical harmonics $Y_{\ell m}$ and Gegenbauer polynomials C_β^α:[16]

$$\mathcal{Y}_{n\ell m}(\hat{x}) = Y_{\ell m}(\hat{r}) \left[\frac{2^{2\ell+1}(n+1)(n-\ell)!\,\ell!^2}{\pi(n+\ell+1)!} \right]^{\frac{1}{2}} C_{n-\ell}^{\ell+1}(\cos\,\Theta)\sin^\ell(\Theta)\,, \tag{3.17}$$

where $\cos\,\Theta = x_4/R$, $\hat{r}$ is the three-space unit vector, and R is the length $R = (|r|^2 + \chi_4^{\,2})^{\frac{1}{2}}$. The functions $\varphi_j(R)$ are radial functions depending only on R and were chosen to be

$$\varphi_j(R) = R^j\, e^{-\alpha R}\,. \tag{3.18}$$

We can expand $\chi^{*}_{k'}(x)$ in the same set of functions, but now with expansion parameters $a'_{\ell',n',j'}$. These functions have been used before by Schwartz[4] and have been applied directly to our problem. The free-wave term has the following expansion in these angular functions:

$$\psi_k{}^0(x) = (2\pi)^2 \sum_{n=0}^{\infty} i^n \frac{J_{n+1}(|k|R)}{|k|\,R} \sum_{\ell=0}^{\infty} \sum_{m=-\ell}^{\ell} \mathcal{Y}^{*}_{n\ell m}(\hat{x})\, \mathcal{Y}_{n\ell m}(\hat{k}) , \tag{3.19}$$

where $\hat{k}$ is the unit four-vector of length $|k|$ in the direction k, and J is the ordinary Bessel function.

Substituting these expansions in the variational principle, Eq.(3.13), and invoking the stationary condition

$$\frac{\delta[T]}{\delta\, a'_{\ell',n',j'}} = 0 , \tag{3.20}$$

we get linear equations for $a_{\ell,n,j}$:

$$\sum_{\substack{\ell=0 \\ n=\ell \\ j=n}} \mathcal{M}_{\ell'n'j',\ell nj}\, a_{\ell nj} = V_{\ell'n'j'} , \tag{3.21}$$

where

$$\mathcal{M}_{\ell'n'j',\ell,n,j} = \int d^4x\, \mathcal{Y}^{*}_{n'\ell'0}(\hat{x})\, \varphi^{*}_{j'}(R)\{\mathcal{D}(\partial_\nu) - V(x)\}\, \mathcal{Y}_{n\ell 0}(\hat{x})\varphi_j(R). \tag{3.22}$$

The ordinary angular momentum ℓ is conserved, and thus we have $\mathcal{M}_{\ell'n'j',\ell nj} = M^{\ell}_{n'j',nj}\,\delta_{\ell\ell'}$. Equations (3.21) are inhomogeneous equations, the corresponding homogeneous equations are precisely those used by Schwartz for the bound-state calculation in reference 4, in which the details for calculating these matrix elements can be found. The inhomogeneous term is

$$V_{\ell nj} = (2\pi)^2\, i^n\, \mathcal{Y}_{n\ell 0}(\hat{k}) \int d^4x\, \frac{J_{n+1}(|k|R)}{|k|R}\, V(x)\, \varphi_j^*(R). \tag{3.23}$$

Defining a partial-wave amplitude

$$T(k',k,E) = \sum_{\ell=0}^{\infty} (2\ell+1)\, t_\ell(|\underset{\sim}{k}'|, k_0', |\underset{\sim}{k}|, k_0, q)\, P_\ell(\cos\theta), \tag{3.24}$$

where $\cos\theta = \underset{\sim}{k}\cdot\underset{\sim}{k}'/(|\underset{\sim}{k}|\,|\underset{\sim}{k}'|)$, we obtain finally

$$t_\ell = \sum_{\substack{n=\ell \\ j=n}} a^*_{\ell nj}\, V_{\ell nj} + B_\ell(k', k_0', k, k_0), \tag{3.25}$$

where

$$B_\ell(k', k_0', k, k_0) = \frac{8\pi^2\lambda}{kk'}\, Q_\ell\left(\frac{k^2 + k'^2 - (k_0 - k_0')^2 + \mu^2}{2kk'}\right) \tag{3.26}$$

and

$$t_\ell(k, 0, k, 0, k) = \frac{8\pi E}{k}\, e^{i\delta_\ell} \sin\delta_\ell\,. \tag{3.27}$$

The integral for the vector term (3.23) was obtained numerically by using a Laguerre integration formula.[16] The standard recursion relations for the Bessel function can be used for recursing down on the index n, and thus not all matrix elements need be calculated from the integral. We chose a sequence of trial functions, letting $n = \ell, \ell + 1, \cdots, N$, and $j = n, n + 1, \cdots, N$ and increased N to see convergence of our results. The matix elements $M^{\ell}_{n',j',nj}$ connect n' only to n and $(n \pm 2)$ and thus the matrix is block-diagonalized into states with $n = \ell, \ell + 2, \cdots,$ and $n = \ell + 1, \ell + 3, \cdots$. In addition $V_{\ell nj}$ is zero for the second set if k_4 is zero. If k'_4 is also zero, only the first set enters in the T matrix, Eq. (3.25). The parameter α was varied and chosen to be the value that gives the fastest convergence.

Table II gives some samples of convergence of $\tilde{t}_\ell = t_\ell - B_\ell$ for S waves. Near threshold the convergence gets bad. For the on-shell case, the convergence also deteriorates near $E = 0$, the onset of the second Born contribution to the left-hand cut. In the neighborhood of a bound state that manifests itself as a pole in t_ℓ, the convergence is also slower, presumably because the pole position itself moves for successive approximations. Except for these special regions the convergence was good.

IV. ANALYTIC CONTINUATION TO THE SCATTERING REGION

The second step in calculating phase shifts is to continue the scattering amplitude to the physical region which is described in this section. We first outline the general method of continuation and then discuss separately the off-mass-shell and on-mass-shell continuations. The latter method was more successful, probably because the function was smoother, i.e. there were fewer nearby singularities. Also the on-shell amplitude satisfies a simple unitarity constraint, and this was used advantageously in the continuation.

A. Method of Analytic Continuation

We chose to do the continuation using a ratio of polynomials for fitting functions. This is the form of a Padé approximant,[17] though we do not determine the coefficients of the polynomials in the canonical way. We find empirically that our fitting functions have properties very similar to Padé approximants.

A Padé approximant is a rational approximation to a function defined in terms of a truncated power series. Consider

$$f(z) = \sum_{i=0}^{J} a_i z^i = \frac{\sum_{i=0}^{M-1} b_i z^i}{1 + \sum_{i=1}^{N-1} c_i z^i} \tag{4.1}$$

where $M + N = J + 2$. The coefficients $\{b_i\}$ and $\{c_i\}$ are determined by demanding that the power-series expansion of the ratio of polynomials coincides with the power-series expansion on the left

for the first $J + 1$ terms. This yields linear equations for $\{b_i\}$ and $\{c_i\}$ as can be seen from the equivalent procedure of multiplying the denominator through and comparing powers of z.

We will be interested in sequences of increasing N for $M = N$. The theory of convergence of such sequences is incomplete in that they appear to converge in much larger demains than can be proven rigorously. Roughly they are found to converge outside the circle of convergence of the power series, the domain being determined by the positions of nonpolar singularities.

For our applications we know the function at a set of points rather than a power series. We still use the Padé form but determine the coefficients by constraining the two forms to be equal at the input points. The equations to determine $\{b_i\}$ and $\{c_i\}$ are

$$\left(1 + \sum_{i=1}^{N-1} c_i z_s^i\right) f(z_s) = \sum_{i=0}^{M-1} b_i z_s^i , \qquad (4.2)$$

where $s = 1, 2, \cdots, M + N - 1$. We will assume that this sequence of approximations converges in a circle that contains the fitting points and excludes all nonpolar singularities. For true Padé approximants this is a conjectured convergence domain. It is possible to find such circles that include the extrapolated points for both continuations discussed below.

Knowing the function at a set of points, Eqs. (4.2) provide the simplest method of computing the coefficients. However, if the function is given at K points there are a large number of ways to choose k of

them for $k < K$ and thus there is no well-defined sequence for judging the convergence of the approximations.

A more elegant method[18] is to map the fitting region into the region $-1 \leqslant z \leqslant +1$ and write the polynomials in the quotient in terms of Legendre polynomials $P_i(z)$:

$$f(z) = \frac{\sum_{i=0}^{M-1} b_i' P_i(z)}{1 + \sum_{i=1}^{N-1} c_1' P_i(z)} \quad . \tag{4.3}$$

The coefficients are determined by multiplying through by the denominator and integrating over the fitting region, which gives

$$M_{j0} + \sum_{i=1}^{N-1} M_{ji} \; c_i' = \sum_{i=0}^{M-1} N_{ji} \; b_i' \; , \tag{4.4a}$$

where

$$M_{ji} = \int_{-1}^{+1} dz \; P_j(z) \; f(z) \; P_i(z) \tag{4.4b}$$

and

$$N_{ji} = \int_{-1}^{+1} P_j(z) \; P_i(z) = \frac{2\delta ij}{2j + 1} \quad . \tag{4.4c}$$

The recursion relation

$$\begin{aligned} i(2j + 1) \, M_{ij} = \; & (2i - 1) \, (j + 1) \, M_{i-1, j+1} \\ & - (2j + 1)(i - 1) \, M_{i-2, j} + (2i - 1)j \, M_{i-1, j-1} \end{aligned} \tag{4.5}$$

enables one to calculate all matrix elements in terms of the matrix elements of the first row and last column.

Equations (4.4) are very similar in form to the equations for true Padé approximants. The coefficients of true Padé approximants are obtained by comparing powers of z, and Eqs. (4.4) are obtained by comparing coefficients of Legendre polynomials. Of course any set of orthogonal polynomials can be used that are appropriate for the particular problem.

One further remark to be made is that the numerator and denominator functions need not be polynomials but can be any sequence of functions with linear parameters. For example it might be desirable to put in known branch points with an appropriate choice of functions. In addition the sequence of functions in the numerator need not be the same as in the denominator.

B. Off-Mass-Shell Continuation

Referring to Fig. 5a, we have as input for the continuation a set of values of $t_\ell(k, 0, k, 0, q)$ for a set of values of q on the positive imaginary axis, for k fixed in the elastic-scattering region. Our object is to continue t_ℓ in q to the point $q = k$. This function is meromorphic in the q plane in a convex region that contains the calculated points on the imaginary axis and the points of interest on the real axis. We set

$$t_\ell(k, 0, k, 0, q) = \frac{\sum_{j=0}^{N-1} a_j(-iq)^j}{1 + \sum_{j=1}^{N-1} b_j(-iq)^j} . \qquad (4.6)$$

Since t_ℓ is real on the imaginary q axis, the coefficients $\{a_i\}$ and $\{b_i\}$ are real. We chose equal powers of q in numerator and denominator because t_ℓ goes to B_ℓ as q approaches ∞. (The Born term B_ℓ is independent of q.) Finally we set $q = k$ to get the phase shift from the expression

$$t_\ell(k, 0, k, 0, k) = \frac{8\pi E}{k} \quad \frac{1}{A + i B} , \tag{4.7}$$

where

$$A = \frac{\tan \delta_\ell}{k} \quad \text{and} \quad B = 1 \ \text{(unitarity)}. \tag{4.8}$$

The accuracy in the calculated value of B serves as a check on the continuation.

The continuation was first done determining the coefficients by point-wise fitting, Eq. (4.2). For a moderately strong attractive potential with a deeply bound state ($\lambda = 3$, $\mu = m = 1$), the results of the continuation were uncertain from 5% to 20% over the elastic region. A great many attempts were made to improve this. These included: determining the coefficients by more sophisticated methods, varying the distribution of input points, trying to improve the accuracy of input numbers, putting known singularities in the fitting functions, generating a power series for t_ℓ in q and then forming true Padé approximants, and continuing in the internal masses. No significant improvement was

was achieved. Schlessinger and Schwartz solved the Schrödinger equation very successfully using this method.[7] There are two principle differences between these two problems: (1) The Bethe-Salpeter amplitude has an infinite number of branch points on the real axis. These include the normal thresholds and a host of others due to our choice of off-mass-shell variables. The Schrödinger amplitude is of course regular on the real q axis. (2) The Bethe-Salpeter equation is two-dimensional in $|\underline{r}|$ and x_4, compared to the one-dimensional Schrödinger radial equation. This fact limits the accuracy which is practical to achieve using the Kohn method. Since simplicity was a desirable element in this calculation, we felt that it would be self-defeating to attempt a more sophisticated solution of the equation. Table III gives a sample of the convergence of the phase shift and "unitarity coefficient" for the off-mass-shell continuation.

It may appear wasteful of computer time in that the function must be calculated at many points to get the phase shift at one point. However, it should be noticed in Eq. (3.21) that k appears only in the inhomogeneous term, and after calculating and inverting the matrix M which depends on E, we can apply its inverse to vectors V with different values of k, which uses a small fraction of the computer time. The continuation time itself is very small.

C. On-Mass-Shell Continuation

Because of the dubious success of the off-mass-shell continuation, a search was made for a smoother function with fewer nearby singularities. The study of the singularity structure of amplitudes leads us to believe

that the on-shell K matrix is the optimum function

$$K_\ell(E^2) = \frac{t_\ell(q, 0, q, 0, q)}{2 - 2i\rho\, t_\ell(q, 0, q, 0, q)} . \tag{4.9}$$

It is well known that $K_\ell(E^2)$ is analytic in E^2 at threshold and has branch points only on the real E^2 axis.

The calculation proceeds as follows: We calculate $t_\ell(q)$ (suppressing the first four arguments) as described in Sec. III, where

$$t_\ell(q) = B_\ell(q) + \tilde{t}_\ell(q) . \tag{4.10}$$

The first Born term $B_\ell(q)$ is known exactly, and $\tilde{t}_\ell(q)$ is calculated numerically. The amplitude t_ℓ and thus $K_\ell(E^2)$ can be found for $4(m^2 - \mu^2) < E^2 < 4m^2$. It is a real analytic function of E^2 with a branch point in this region at $E^2 = 4m^2 - \mu^2$ coming from $B_\ell(q)$. We can then expand the domain of analyticity further by removing the cut contribution to $K_\ell(E^2)$ for $4(m^2 - \mu^2) < E^2 < 4m^2 - \mu^2$. Define

$$\tilde{K}_\ell(E^2) = K_\ell(E^2) - K_\ell^{\,\mathrm{cut}}(E^2) , \tag{4.11}$$

where

$$K_\ell^{\,\mathrm{cut}}(E^2) = \frac{1}{\pi} \int_{4(m^2-\mu^2)}^{4m^2-\mu^2} dE'^2 \; \frac{\Delta K_\ell(E'^2)}{E'^2 - E^2} \tag{4.12}$$

and

$$\Delta K_\ell(E^2) = \frac{1}{2i} [K_\ell(E^2 + i\epsilon) - K_\ell(E^2 - i\epsilon)] . \qquad (4.13)$$

The function $\tilde{K}_\ell(E^2)$ is analytic on the real axis in the region $4(m^2 - \mu^2) < E^2 < (2m + \mu)^2$. This function was continued to the scattering region using the Legendre fit, Eq. (4.4), in the variable E^2, and then the cut contribution $K_\ell^{cut}(E^2)$ was added back in. The phase shift was found from the formula

$$K_\ell(E^2) = \frac{4\pi E}{k} \tan \delta_\ell . \qquad (4.14)$$

The results compared quite favorably with those of Schwartz and Zemach for moderately strong potentials.[2] The relative errors in the phase shifts for various potentials are plotted in Fig. 6. In the region of E^2 between zero and four, the relative error of t_ℓ is plotted. We see that on the average about two significant digits are lost in the extrapolation. The errors in both the input numbers and phase shifts increase for stronger potentials. A sample of convergence can be found in Ref. 8, Table I.

D. Comparison

A comparison of the results calculated in these two ways serves to point out that the continuation will be more successful when there are fewer nearby singularities to contend with. Padé approximants represent branch cuts by a line of poles. It is important to get a

good representation of the function for lower orders of fitting functions, because cancellations in the fitting procedure limit the practical number of fitting parameters for the accuracy of our input numbers. Also convergence or stability of the extrapolated numbers must be observed when the number of parameters is increased.

We can estimate from considering Fig. 5a that possibly five poles are necessary to represent the nearby cuts of the off-shell amplitude. This means we have eleven parameters in our functions. On the other hand, the nearby cuts in the on-shell amplitude $\tilde{K}_\ell(E^2)$ could probably be represented by two poles, one in the elastic region and one on the left-hand cut. Of course, the presence of bound states further increases the number of poles necessary to get a good representation. For stronger potentials the input numbers are less accurate, there are more nearby bound-state poles, and the discontinuities across the nearby cuts are larger.

ACKNOWLEDGMENTS

I am pleased to thank Professor Charles Schwartz for suggesting this problem and for his guidance and encouragement. I am also indebted to Professor Charles Zemach for initiating my work on the Bethe-Salpeter equation which led to this research, and to Dr. Leonard Schlessinger for helpful discussions on the numerical continuation procedure. I would also like to express my appreciation to William Kaufmann and Dr. Klaus Rothe for many discussions throughout the course of this work.

APPENDIX: ELASTIC THRESHOLD BRANCH POINT

In this appendix we show that the elastic-threshold branch point of the partial-wave Bethe-Salpeter amplitude is two-sheeted in ω^2 for both legs off the mass-shell. It is well known that this is the case for the on-shell amplitude. It is implicit in the paper of Levine et al.[3] that the singly off-shell T matrix has this property. We will generalize this result to the doubly off-shell T matrix following the methods of Kowalski.[19]

It can be shown that each term in the Born series is two-sheeted at threshold (except the first which is independent of ω^2), and if the Born series converges, then it follows that the partial-wave amplitude is also two-sheeted. We prefer to work with the integral equation for the sake of elegance, so as not to have to rely on the convergence of the Born series. It is of course possible to have anamolous thresholds coming through the normal threshold onto the physical sheet. This occurs as the external masses are increased and arises from pinches between the Green's-function poles and the potential singularities. However if we are not too far off-mass-shell, the only pinch that occurs is between the Green's-function poles for small q. It is this pinch that we are studying.

Levine et al.[3] defined a new function f_ℓ through the equation

$$T_\ell(k', k_0', q, 0, \omega) = f_\ell(k', k_0', q, 0, \omega)\, T_\ell(q, 0, q, 0, \omega) . \quad (A.1)$$

The function f_ℓ clearly has the property

$$f_\ell(q, 0, q, 0, \omega) = 1 . \tag{A.2}$$

Substituting this in the Bethe-Salpeter equation, we arrive at a formula for the on-shell T matrix

$$T_\ell(q) = B_\ell^{(1)}(q) \left[1 + \int_0^\infty dp \int_{-\infty}^\infty dp_0 \, B_\ell^{(1)}(q, 0, p, p_0) \, G_\omega(p, p_0) \times f_\ell(p, p_0, q, 0, \omega) \right]^{-1}, \tag{A.3}$$

where all arguments except q are suppressed for fully on-shell quantities. The integral equation for f_ℓ is

$$f_\ell(k', k_0', q, 0, \omega) = \frac{B_\ell^{(1)}(k', k_0', q, 0)}{B_\ell^{(1)}(q)} + \int_0^\infty dp \int_{-\infty}^\infty dp_0 \, M(k_0', k, p, p_0, \omega) \, G_\omega(p, p_0) \, f_\ell(p, p_0, q, 0, \omega), \tag{A.4}$$

where

$$M(k_0', k', p, p_0, \omega) = \frac{B_\ell^{(1)}(k', k_0', q, 0) \, B_\ell^{(1)}(p, p_0, q, 0)}{B_\ell^{(1)}(q)} - B_\ell^{(1)}(k', k_0', p, p_0). \tag{A.5}$$

The advantage of introducing the function f_ℓ is that it does not have a threshold branch point, as we will show. The T matrix is

calculated through the formulae (A.3) and (A.1), the branch point coming from a pinch in the integral.

Consider an integral of the form

$$I = \int_{-\infty}^{\infty} dp \int_{-\infty}^{\infty} dp_0 \; H(p, p_0, \omega) \; G_\omega(p, p_0), \qquad (A.6)$$

where $H(p, p_0, \omega)$ is even in p, which allows us to symmetrize the p integration, and the function H depends only on q^2 in the neighborhood of threshold. Integrals (A.3) and (A.4) are of this form. This follows from the fact that $\chi_\ell(k', k_0', k, k_0, \omega) = (-)^{\ell+1}\chi_\ell(-k', k_0', k, k_0, \omega)$, where χ_ℓ is T, f, M or $B^{(1)}$. The same relation holds for the right leg. The Green's function has four poles in the p_0 plane--two in the upper half and two in the lower half. The p_0 contour is on the real axis. Distort the contour into the upper-half plane as shown in Fig. 7a to Γ_{p_0} picking up the residues of the poles. The integral can be written

$$I = \int_{-\infty}^{\infty} dp \int_{\Gamma_{p_0}} dp_0 - \frac{1}{16\pi i\omega} \int_{-\infty}^{\infty} \frac{dp}{(p^2+m^2)^{\frac{1}{2}}} \left\{ \frac{H\left(p, \omega - (p^2+m^2)^{\frac{1}{2}}, \omega\right)}{\omega - (p^2+m^2)^{\frac{1}{2}}} + \frac{H\left(p, -\omega-(p^2+m^2)^{\frac{1}{2}}, \omega\right)}{\omega + (p^2+m^2)^{\frac{1}{2}}} \right\}. \qquad (A.7)$$

The integral along Γ_{p_0} experiences no pinches and is regular at $\omega^2 = m^2$. The integrand of the p integral has singularities at $p = \pm q$ as shown in Fig. 7b. The pinching between these two poles

gives the threshold branch point at $q = 0$. Passing the p contour to Γ_p (Fig. 7b) we arrive at

$$I = \int_{-\infty}^{\infty} dp \int_{\Gamma_{p_0}} dp_0 + \int_{\Gamma_p} dp + \frac{m}{8\pi^2 \omega^2 q} [H(q, 0, \omega)] . \quad (A.8)$$

The first two integrals are regular in q^2 at threshold, and the second integral is q times an even function of q, thus exhibiting the two-sheeted branch point.

These considerations apply for Eq. (A.3) and the Born series of Sec. II. However, for the integral equation for f_ℓ in (A.4) we have $H(q, 0, \omega) = 0$. The function M has zeros just so as to cancel the poles that produce the pinches, and thus f has no threshold branch point.

The generalization to both legs off the mass-shell has been carried out by Kowalski[19] for the Schrödinger equation and generalizes immediately to the Bethe-Salpeter equation. The generalized form of Eq. (A.1) is

$$T_\ell(k', k_0', k, k_0, \omega) = f_\ell(k', k_0', q, 0, \omega)\, T_\ell(q)\, f_\ell(k, k_0, q, 0, \omega)$$

$$+ f_\ell(k', k_0', k, k_0, \omega)\, B_\ell^{(1)}(q) - f_\ell(k', k_0', q, 0, \omega)\, B_\ell^{(1)}(k, k_0, q, 0). \quad (A.9)$$

This reduces to Eq. (A.1) for the right leg on-mass-shell. For the left leg only on-mass-shell we obtain

$$f_\ell(q,\ 0,\ k,\ k_0,\ \omega) \ = \ \frac{B_\ell^{(1)}(k,\ k_0,\ q,\ 0)}{B_\ell^{(1)}\ (q)} \ . \qquad \text{(A.10)}$$

Note that f_ℓ is not symmetric in its right and left legs.

The arguments go through just as before: Eq. (A.9) gives the off-shell T matrix in terms of the on-shell T and f , Eq. (A.3) still gives the on-shell T in terms of f, but the integral equation for f is now

$$f_\ell(k',\ k_0',\ k,\ k_0,\ \omega) \ = \ \frac{B_\ell^{(1)}\ (k',\ k_0',\ k,\ k_0)}{B_\ell^{(1)}\ (q)}$$

$$+ \int_0^\infty dp \int_{-\infty}^\infty dp_0\ M(k',k_0',p,p_0,\omega)\ G_\omega(p,p_0)\ f(p,p_0,k,k_0,\omega) \ . \qquad \text{(A.11)}$$

FOOTNOTES AND REFERENCES

* This work was done under the auspices of the United States Atomic Energy Commission.

† Present address: Department of Physics, University of California, Santa Barbara, California.

1. E. E. Salpeter and H. A. Bethe, Phys. Rev. 84, 1232 (1951).

2. C. Schwartz and C. Zemach, Phys. Rev. 141, 1454 (1966).

3. M. J. Levine, J. Wright, and J. A. Tjon, Phys. Rev. 154, 1433 (1967).

4. C. Schwartz, Phys. Rev. 137, B717, (1965).

5. P. R. Graves-Morris, Phys. Rev. Letters 16, 201 (1966).

6. A. Pagnamenta and J. G. Taylor, Phys. Rev. Letters 17, 218 (1966).

7. L. Schlessinger and C. Schwartz, Phys. Rev. Letters 16, 1173 (1966).

8. R. Haymaker, Phys. Rev. Letters, 18, 968 (1967).

9. A discussion of the singularity structure of the full amplitude in the integration variables can be found in Ref. 6.

10. A discussion of singularities of multiple integrals can be found in R. J. Eden, P. V. Landshoff, D. I. Olive, and J. C. Polkinghorn, The Analytic S Matrix (Cambridge University Press, New York, 1966).

11. Ibid., p. 62.

12. For a discussion of the hierarchy of singularities of Feynman diagrams and the contraction scheme see Ref. 10, Sec. 2.2.

13. G. C. Wick, Phys. Rev. 96, 1124 (1954).

14. See Ref. 2, Sec. II.D.

15. Ibid., Sec. IV.C.

16. Our formulas are taken from M. Abramowitz and I. Stegun, Handbook of Mathematical Functions (Dover Publications, Inc., New York, 1965). Some formulae are given concisely in Ref. 4.

17. H. Padé, Thesis, Ann. Ecole Norm. 9, Suppl. 1 (1892). See also G. Baker's article in Advances in Theoretical Physics, Vol. 1 (Academic Press, New York, 1965) and H. S. Wall, Analytic Theory of Continued Fractions (Van Nostrand, Princeton, New Jersey, 1948).

18. I am indebted to Dr. Leonard Schlessinger, University of Illinois, Urbana, for this method.

19. K. Kowalski, Phys. Rev. Letters 15, 798 (1965).

TABLE I. Singular surfaces of the Bethe-Salpeter second Born term $B_{\ell}^{(2)}(k', k_0', k, k_0, \omega)$ classified according to the number of singular surfaces, $S_i = 0$, of the integral participating.

No. of surfaces	Singular surfaces Participating in integrand	Singular Surface in Integral	
1	S_1, S_2, S_3, S_4 S_5, S_6	$\mu^2 = 0$	(1)
		$m^2 = 0$	(2)
2	$S_1 S_3, S_2 S_4$	$(k - k')^2 - (k_0 - k_0')^2 + 4\mu^2 = 0$	(3)
	$S_1 S_4, S_2 S_3$	$(k + k')^2 - (k_0 - k_0')^2 + 4\mu^2 = 0$	(4)
	$S_5 S_6$	$\omega^2 = m^2$	(5)
	$S_1 S_5, S_2 S_5$	$k^2 - (k_0 - \omega)^2 + (\mu + m)^2 = 0$	(6)
	$S_1 S_6, S_2 S_6$	$k^2 - (k_0 + \omega)^2 + (\mu + m)^2 = 0$	(7)
	$S_3 S_5, S_4 S_5$	$k'^2 - (k_0' - \omega)^2 + (\mu + m)^2 = 0$	(8)
	$S_3 S_6, S_4 S_6$	$k'^2 - (k_0' + \omega)^2 + (\mu + m)^2 = 0$	(9)
3	$S_1 S_5 S_6, S_2 S_5 S_6$	$[(k-q)^2 - k_0^2 + \mu^2][(k+q)^2 - k_0^2 + \mu^2] = 0$	(10)
	$S_3 S_5 S_6, S_4 S_5 S_6$	$[(k'-q)^2 - k_0'^2 + \mu^2][(k'+q)^2 - k_0'^2 + \mu^2] = 0$	(11)
	$S_1 S_3 \begin{pmatrix} S_5 \\ S_6 \end{pmatrix}, S_2 S_4 \begin{pmatrix} S_5 \\ S_6 \end{pmatrix}$	$[(k'^2 - (k_0' \mp \omega)^2 + \mu^2 - m^2)(k_0 \mp \omega) - (k^2 - (k_0 \mp \omega)^2 + \mu^2 - m^2)(k_0' \mp \omega)]^2$ $-[(k'^2 - (k_0' \mp \omega)^2 + \mu^2 - m^2)\, k - (k^2 - (k_0 \mp \omega)^2 + \mu^2 - m^2)\, k']^2$ $+ 4[k'(k_0 \mp \omega) - k(k_0' \mp \omega)]^2 m^2 = 0$	(12)
	$S_1 S_4 \begin{pmatrix} S_5 \\ S_6 \end{pmatrix}, S_2 S_3 \begin{pmatrix} S_5 \\ S_6 \end{pmatrix}$	Eq. (12) with $k \to -k$	(13)

TABLE II. Sample of convergence of the variational calculation of $\tilde{t}_\ell(k,0,k,0,q)$ for $\lambda = 3$, $\mu = m = 1$, $\ell = 0$. Off-shell $k^2 = 0.4m^2$; On-shell $k^2 = (E^2/4) - m^2$. For both cases, the convergence is better for weaker potentials and for repulsive potentials. The sign change is due to a bound state at $E^2 \approx 1$.

	Off-shell $\tilde{t}_\ell(k,0,k,0,q)$			On-shell $\tilde{t}_\ell(q,0,q,0,q)$		
No. of Basis Functions	$E^2 = 3.8603$ $\alpha = 0.35$	$E^2 = 2.8165$ $\alpha = 0.9$	$E^2 = -0.870615$ $\alpha = 2.2$	$E^2 = 3.5$ $\alpha = 0.7$	$E^2 = 2.0$ $\alpha = 1.3$	$E^2 = 0.5$ $\alpha = 1.1$
2	-626.6	-815.29	372.939	-899.7	-2364.08	6403.1
4	-474.1	-733.28	608.182	-761.9	-2148.71	6492.3
6	-470.7	-708.67	707.085	-752.9	-2034.14	6992.4
9	-444.3	-702.01	723.856	-736.0	-2017.33	6995.8
12	-444.1	-698.42	727.655	-732.5	-2009.96	7035.2
16	-435.7	-697.53	727.968	-729.4	-2007.84	7036.7
20	-434.9	-696.93	728.079	-728.2	-2007.11	7045.1
25	-431.4	-696.77	728.086	-727.5	-2006.77	7045.7
30	-430.9	-696.64	728.092	-727.1	-2006.66	7048.5
36	-429.3	-696.60	728.095	-726.9	-2006.59	7048.7

TABLE III. Samples of the stability of the extrapolation for the off-mass-shell continuation for $m = \mu = 1$.

Padé Approximant	$\lambda = 1$, $E^2 = 4.4$		$\lambda = 1$, $E^2 = 5.6$		$\lambda = 3$, $E^2 = 5.2$	
	Unitarity	δ_0/π	Unitarity	δ_0/π	Unitarity	δ_0/π
2, 2	0.979	0.526	1.091	0.328	1.23	0.725
3, 3	0.978	0.528	1.085	0.327	1.17	0.714
4, 4	1.049	0.496	0.972	0.3341	1.09	0.699
5, 5	1.107	0.515	0.966	0.3336	1.09	0.692
6, 6	1.079	0.495	0.976	0.3344	1.10	0.703
7, 7	1.026	0.512	0.970	0.3347	1.21	0.694
8, 8	1.064	0.506	0.971	0.3345	1.08	0.699
S. Z.[a]	1.0	0.49865	1.0	0.34613	1.0	0.72906

a. These values (C. Schwartz, private communication) were calculated using the method of Ref. 2.

FIGURE LEGENDS

Fig. 1. (a) Some singular surfaces of the integrand for the Bethe-Salpeter second Born term $B_\ell^{(2)}(k',k_0',k,k_0,\omega)$ for $\omega^2 > m^2$. S_2, S_3, and S_4 were left out for the sake of clarity. (b) Singularities of (a) in the p_0 complex plane for fixed real p.

Fig. 2. The box diagram and some pertinent contracted diagrams with singularities independent of $\cos\theta$. The sheet structure of singularities for cases (c) and (d) are shown.

Fig. 3. Some singularities of the Bethe-Salpeter second Born term $B_\ell^{(2)}(k',k_0',k,k_0,\omega)$ as a function of the left-leg variables k', k_0'. The subscripts on T refer to the surfaces S_i that are responsible for it. The disappearance of a three-surface singularity $T_{1,5,6}$ on other sheets of two-surface singularities $T_{1,5}$ and $T_{1,6}$ is shown. For the case drawn, $m^2 < \omega^2 < (m+\mu)^2$. The surfaces given by Eqs. (3) and (4) of Table I were omitted for the sake of clarity. The singularities given by Eqs. (12) and (13) do not intersect the real k', k_0' plane for the chosen right-leg variables k, k_0. (b) k_0' plane for $k' \lesssim q$.

Fig. 4. Singularities of the Bethe-Salpeter second Born term in the q plane for $k_0 = k_0' = 0$. (a) $k = k'$ fixed in the scattering region. (b) $k = k' = q$.

Fig. 5. Important singularities of $B_\ell^{(N)}(k',k_0',k,k_0,\omega)$ in the q plane for $k_0 = k_0' = 0$, in the variables of Fig. 4. (a) The normal thresholds lie on the positive and negative real q axis. There are many more singularities than just normal thresholds on the

real axis, e.g. the surface $T_{1,3,5}$ of Fig. 4 and its offspring in higher Born terms for q sufficiently larger than k. There are also branch points at $q = -\sigma i \mu/2$, $\sigma = 1,2,\cdots,(N-2)$, and $q = -i m$, which were omitted for the sake of clarity.

(b) In the on-mass-shell variable $q = k = k'$, only normal thresholds are on the real axis. T_i is the ith threshold.

Fig. 6. Relative errors incurred in the calculation of phase shifts using the on-mass-shell continuation. The variational calculation was done in the region $0 < E^2 < 3.5$ and the errors indicate the quality of the input numbers for the extrapolation. The extrapolated region is for $E^2 > 4$.

Fig. 7. Contour distortions for integrations generating the threshold branch point by pinching of Green's function poles (marked x).

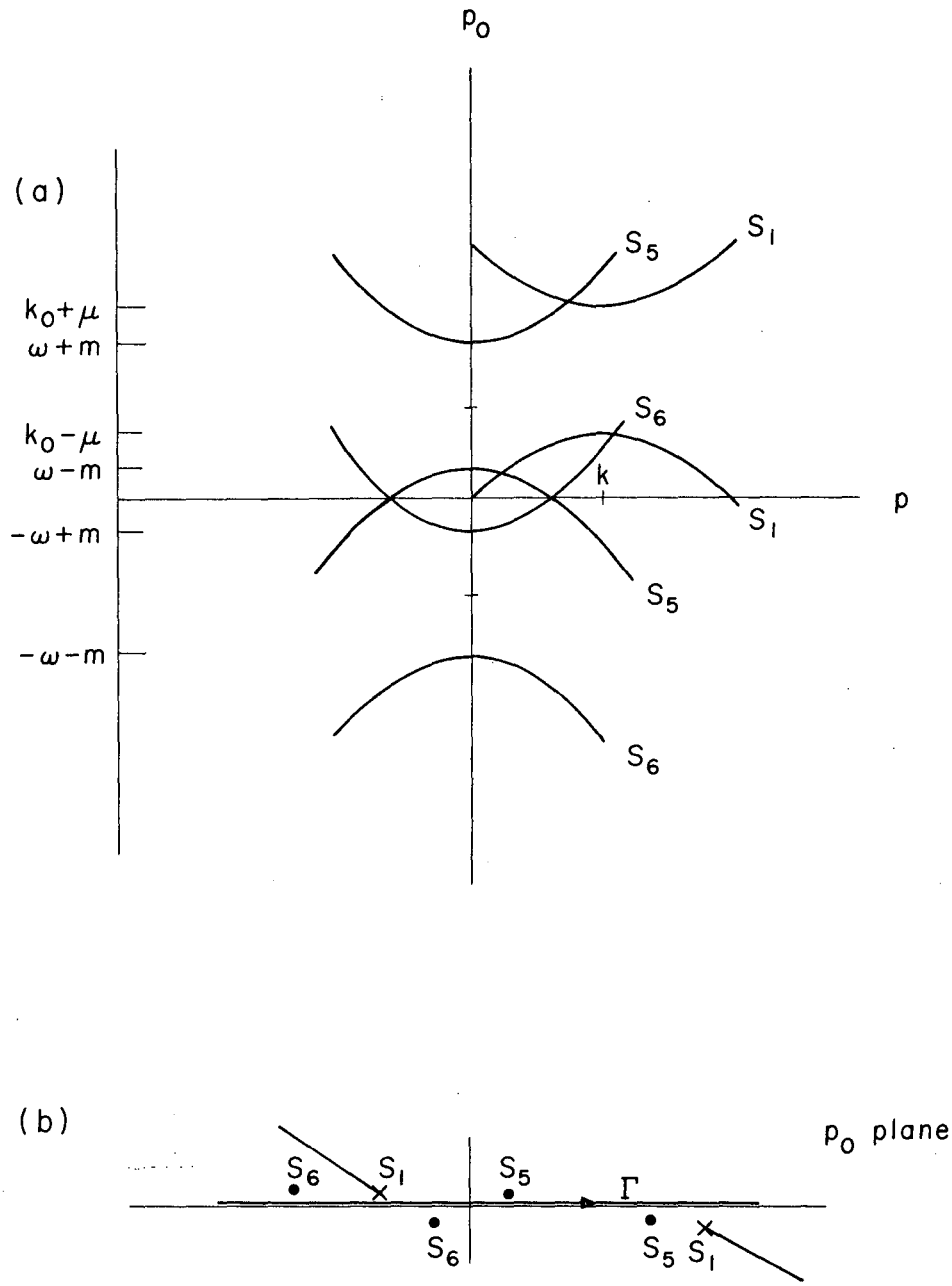
(a)
p_0
$k_0+\mu$
$\omega+m$
$k_0-\mu$
$\omega-m$
$-\omega+m$
$-\omega-m$
S_5
S_1
S_6
k
p
S_1
S_5
S_6
(b)
p_0 plane
S_6
S_1
S_5
Γ
S_6
S_5
S_1
XBL677-3370

Fig. 1

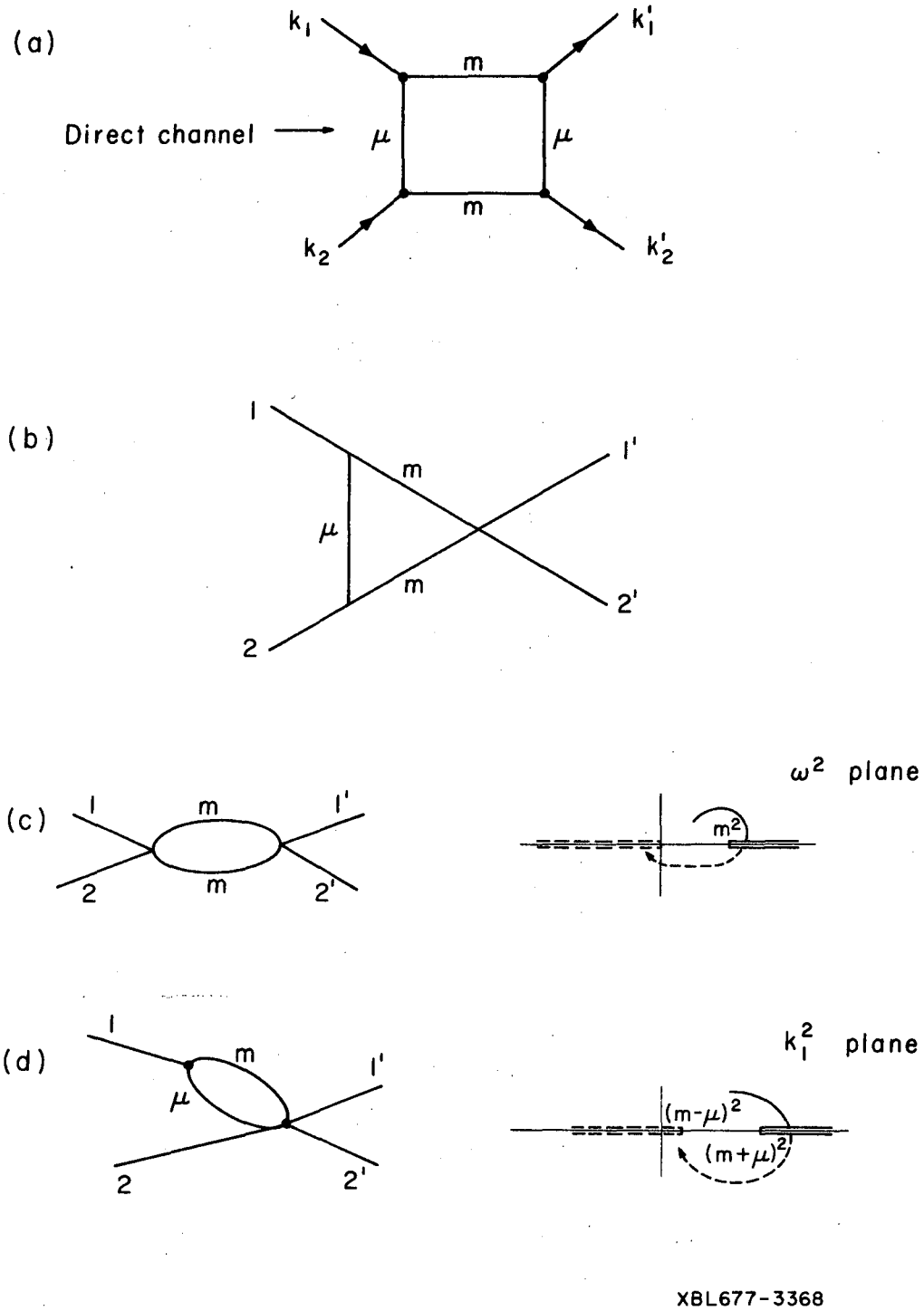
(a)
Direct channel
k_1
k_1'
k_2
k_2'
m
m
μ
μ
(b)
1
1'
2
2'
m
m
μ
(c)
1
1'
2
2'
m
m
ω^2 plane
m^2
(d)
1
1'
2
2'
m
μ
k_1^2 plane
$(m-\mu)^2$
$(m+\mu)^2$
XBL677-3368

Fig. 2

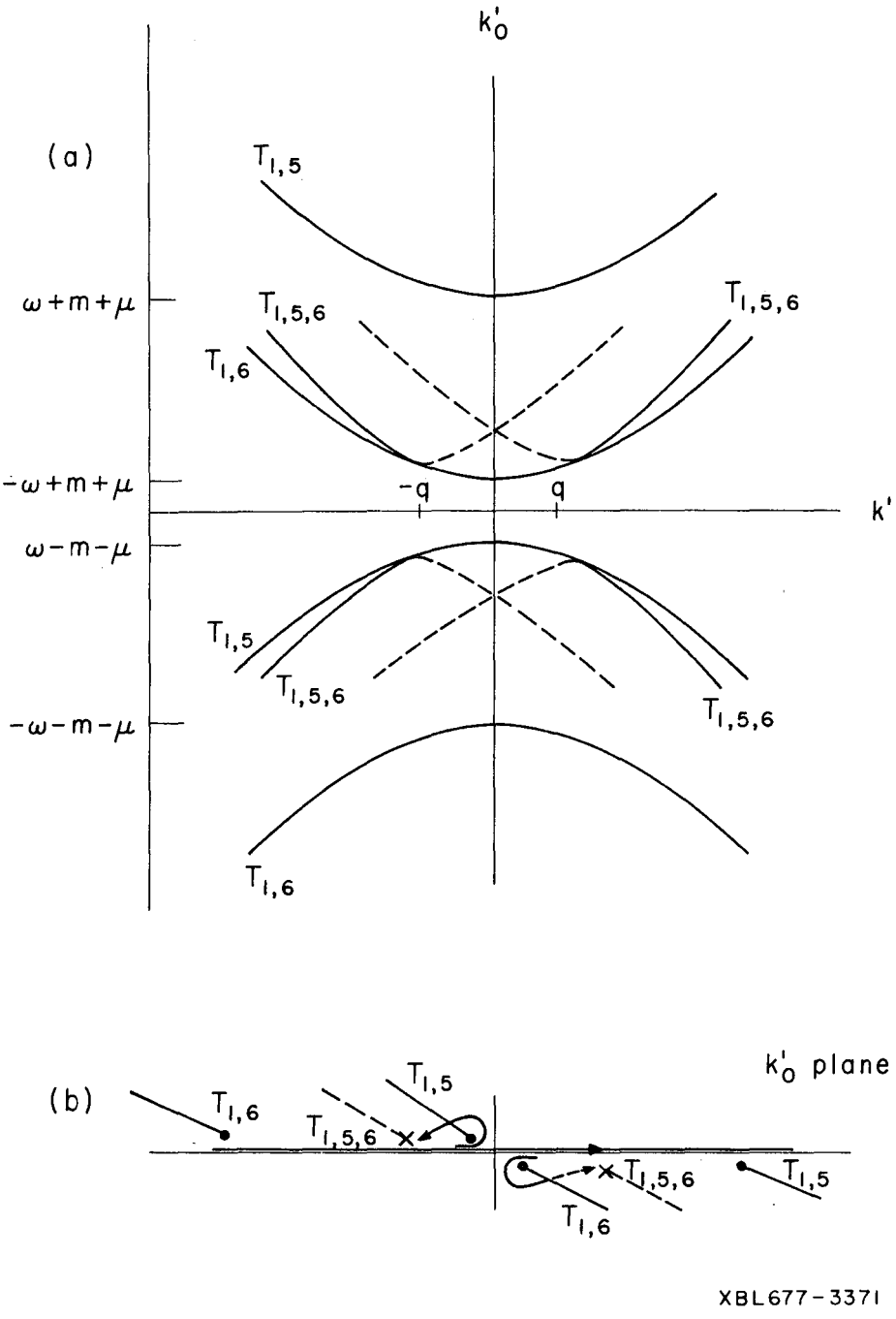
(a)
k'_0
$T_{1,5}$
$\omega+m+\mu$
$T_{1,5,6}$
$T_{1,6}$
$T_{1,5,6}$
$-\omega+m+\mu$
$-q$
q
k'
$\omega-m-\mu$
$T_{1,5}$
$T_{1,5,6}$
$T_{1,5,6}$
$-\omega-m-\mu$
$T_{1,6}$
(b)
k'_0 plane
$T_{1,5}$
$T_{1,6}$
$T_{1,5,6}$
$T_{1,5,6}$
$T_{1,5}$
$T_{1,6}$
XBL677-3371

Fig. 3

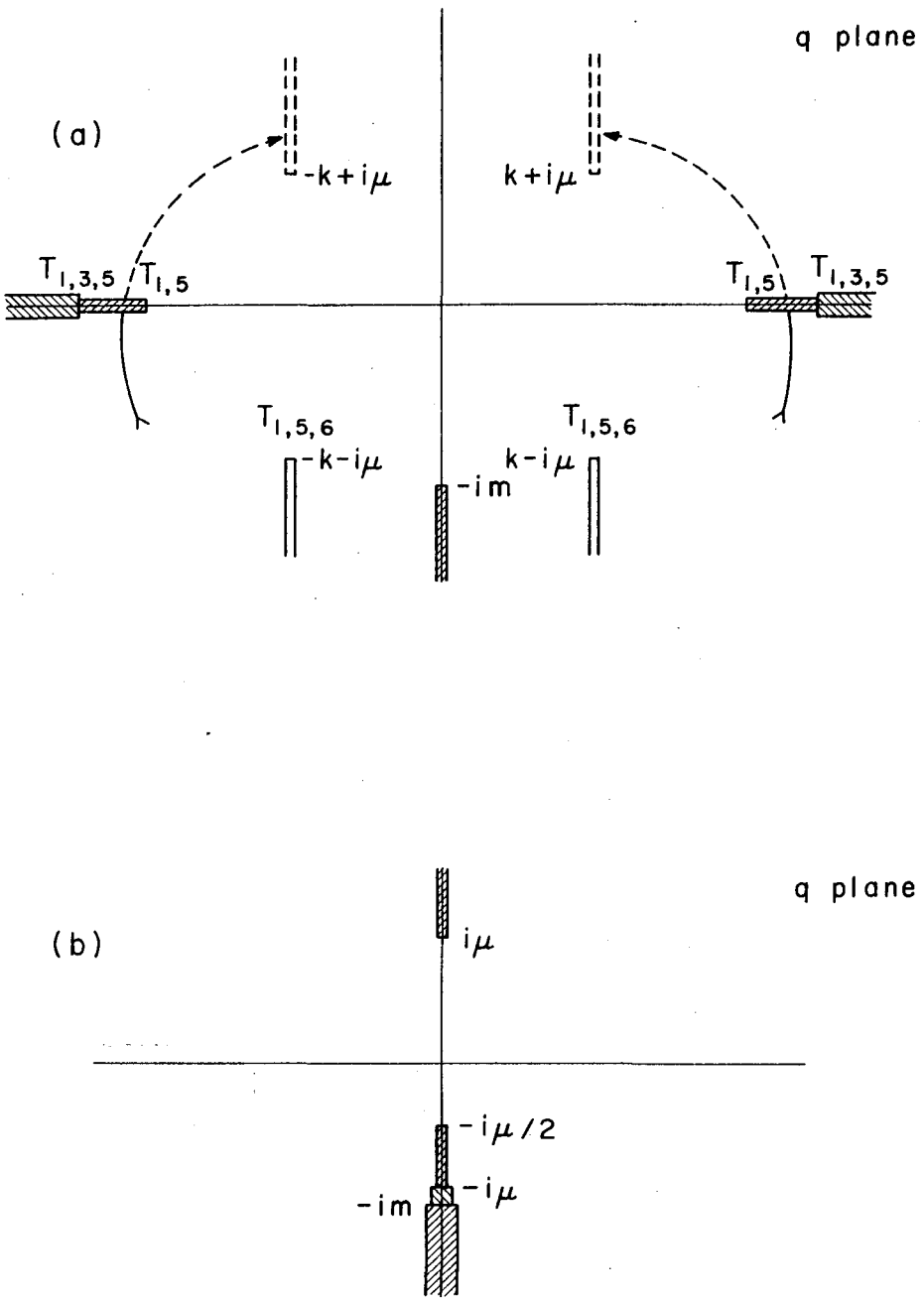
q plane
(a)
-k+iμ
k+iμ
T1,3,5
T1,5
T1,5
T1,3,5
T1,5,6
T1,5,6
-k-iμ
k-iμ
-im
q plane
(b)
iμ
-iμ/2
-im
-iμ
XBL677-3372

Fig. 4

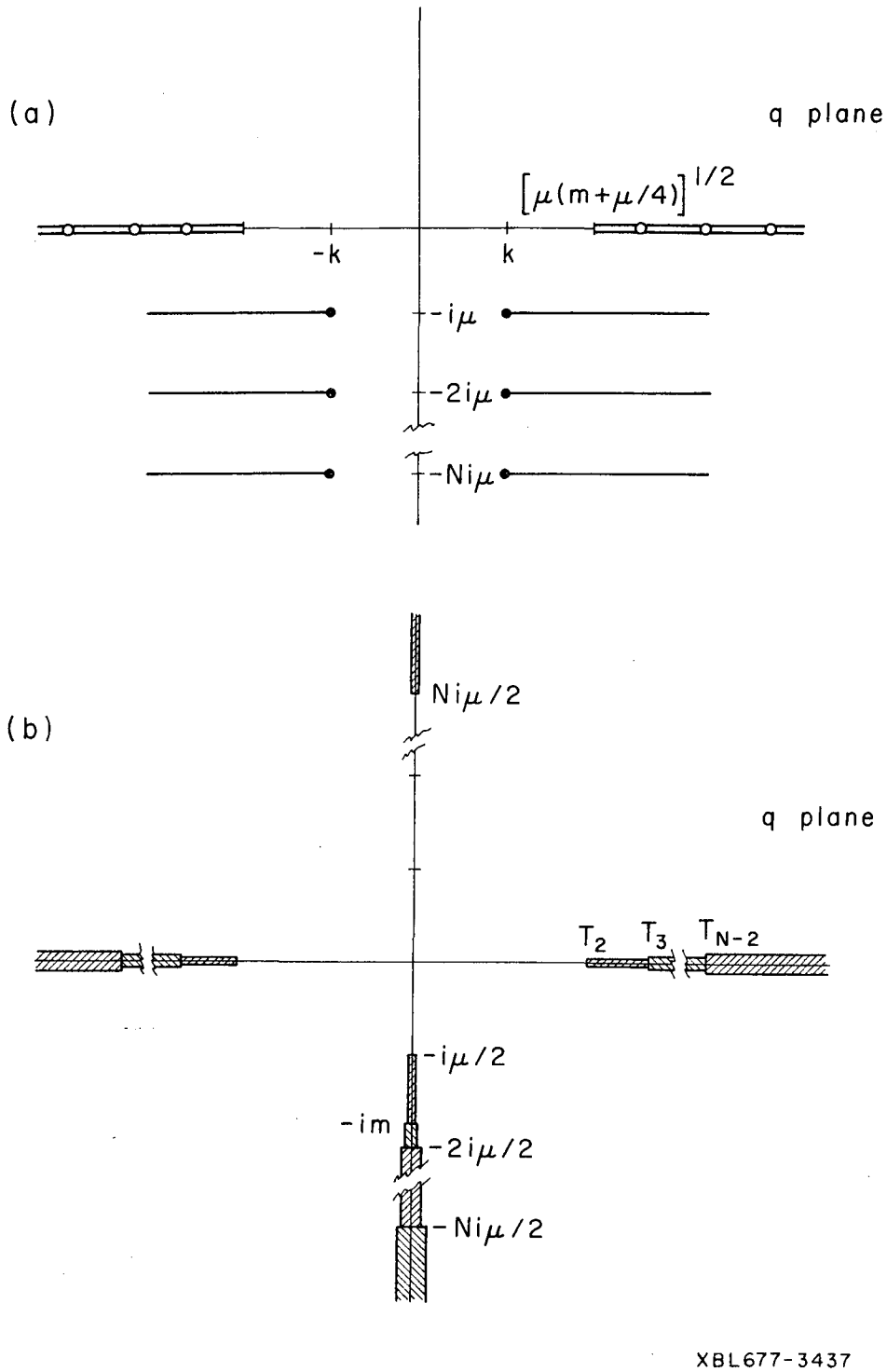
(a)
q plane
$[\mu(m+\mu/4)]^{1/2}$
-k
k
$-i\mu$
$-2i\mu$
$-Ni\mu$
(b)
$Ni\mu/2$
q plane
T_2
T_3
T_{N-2}
$-i\mu/2$
$-im$
$-2i\mu/2$
$-Ni\mu/2$
XBL677-3437

Fig. 5

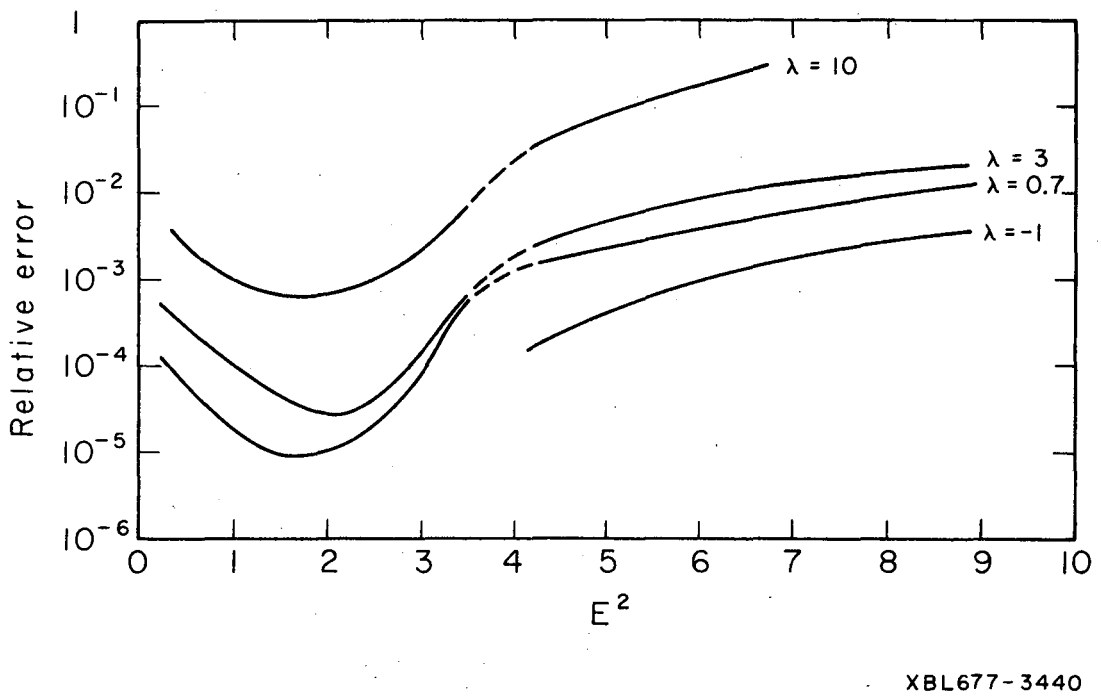
Relative error
1
10^{-1}
10^{-2}
10^{-3}
10^{-4}
10^{-5}
10^{-6}
0 1 2 3 4 5 6 7 8 9 10
E^2
λ = 10
λ = 3
λ = 0.7
λ = -1
XBL677-3440

Fig. 6

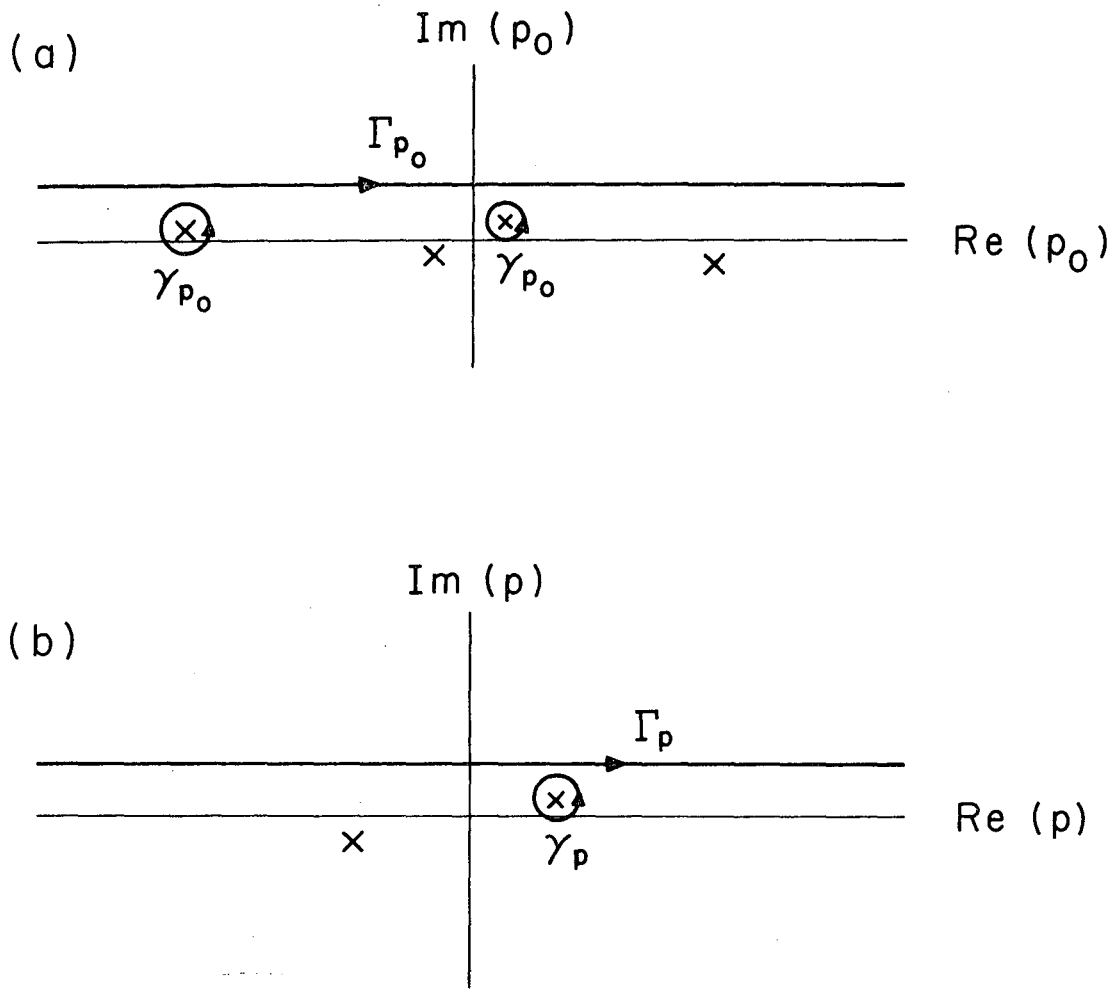

XBL677-3442

Fig. 7